Microstructure Peculiarities and Electromechanical Properties of Porous Piezoceramics

Natalia A. Shvetsova, Igor A. Shvetsov, Ekaterina I. Petrova, Andrey V. Nasedkin, and Andrey N. Rybyanets(✉)

Institute of Physics, Southern Federal University, Rostov-On-Don, Russia
arybyanets@gmail.com

Abstract. In this paper, a comprehensive study of microstructure peculiarities and electromechanical properties of porous piezoceramics based on PZT compositions was performed. Experimental samples of porous piezoceramics were fabricated using a modified method of burning-out a pore formers. Porosity dependencies of elastic, dielectric, and electromechanical parameters of the porous piezoceramics in the relative porosity range of 0–50% were measured and analyzed. Full set of complex constants of porous ceramics with different porosity and their frequency dependences were measured using the piezoelectric resonance analysis method. The microstructural and physical mechanisms of elastic losses and dispersion in porous piezoceramics were considered. In conclusion, microstructure/properties interrelations, as well as new applications of porous piezoceramics were discussed.

Keywords: Porous piezoceramics · Microstructure · Piezoceramic skeleton · Electromechanical properties · Elastic dispersion · Elastic losses · Complex constants · Piezoelectric resonance analysis

1 Introduction

The active use of composite materials in ultrasonic transducers and their production requires the solution of many technological problems, in particular, the revision of the fundamental views of designers and technologists of piezoceramic materials [1]. One of the relatively new promising piezoelectric materials is porous piezoceramics [2, 3].

Porous ceramics are heterogeneous media with unique microstructures that provide original, effective properties on which many different applications are based [4–6]. In particular, porous ceramics combine general characteristics, associated with the geometry and topology of porous microstructures, with the characteristic properties of ceramics as a specific class of materials. It is obvious that the use of porous ceramics is based on the structural and functional properties and characteristics, caused by microstructure, the latter being determined by the initial raw material, composition and method of the fabrication of ceramics.

It was shown that the porous ceramics technology results in increasing of piezoelectric anisotropy, removal of internal mechanical stresses, increasing in mechanical

I. A. Parinov et al. (Eds.): *Physics and Mechanics of New Materials and Their Applications*, SPM 20, pp. 175–188, 2023. https://doi.org/10.1007/978-3-031-21572-8_15

durability, preventing of cracking and finally, allows production of stable in time elements of such "technologically difficult" ceramics as lead titanate and lead metaniobate with excellent and reproducible properties [7, 8]. Various combinations of basic preparation methods can be used to create hierarchical microstructures with a wide range of pore sizes and/or different pore space topologies at different length scales [9–11]. All of these factors must be considered when selecting the appropriate porous ceramic technology for the microstructure, properties and application requirements.

Intensive R&D and technological works, as well as the development of new manufacturing methods allowed organizing the mass production of porous piezoceramics with controlled and reproducible porosity and electromechanical properties [12, 13]. Porous piezoceramics, based on different piezoceramic compositions, are widely used now in ultrasonic transducers and sensors for various technical applications such as medical ultrasonic devices, nondestructive testing, underwater acoustics, and others [14–16]. In particular, porous piezoceramics, based on various piezoceramic compositions, have been proposed as a replacement for lead methaniobate for use in broadband ultrasonic transducers [17, 18]. However, despite numerous studies and long observation, regarding porosity effects on material properties, many aspects of the relationship between the microstructure peculiarities and electromechanical parameters of porous piezoceramics are still unclear. Moreover, the reasons for the frequency dependences of the complex parameters, as well the microstructural and physical mechanisms of elastic losses and dispersion in porous piezoceramics seem not yet clear.

In this work, we studied the microstructure peculiarities and electromechanical properties as well as elastic dispersion and losses in porous ferroelectric ceramics, based on the PZT system.

2 Objects of the Study and Methods of Measurements

Ferroelectrically "soft" PZT-type piezoelectric ceramics of the composition $PbTi_{0.45}Zr_{0.53}(W_{1/2}Cd_{1/2})_{0.02}O_3$ with different relative porosity in the range of 0–50% and average pore size of 10–30 μm were chosen as the object of the study. Experimental samples of porous piezoceramics were obtained using a modified method of pore formers burning-out [7]. Porosity and pore size distribution were determined using simple but effective methods of stereology and hydrostatic weighing, as well as from the results of weighing and measuring the geometric dimensions of a porous piezoceramic sample, followed by calculation of the relative porosity, using the formula: $p = (p_{theor.} - p_{exp.})/p_{theor}$, where $p_{theor.}$ is the X-ray density of dense piezoceramics and $p_{exp.}$ is the measured density of porous piezoceramics.

Thin discs (Ø 20 mm, thickness of 1 mm), rectangular plates ($20 \times 10\ mm^2$, thickness of 1 mm) and long rods (Ø 1 mm, length of 6 mm) of porous piezoceramics were used for the experiments. The porous ceramics samples with vacuum deposited Cr/Ni electrodes were poled in air by applying to the electrodes a DC electric field (~1 kV/mm) at heating above Curie temperature (~340 °C) and then cooling to room temperature.

Microstructural studies were performed on polished and chipped surfaces of porous piezoceramics samples using the scanning electron microscopes (JEOL JSM-6390LA and TM-100, Hitachi).

Piezoresonance spectra measurements for radial, length-extensional, and thickness modes of vibrations were made using Agilent 4294A impedance analyzer. The measurements were carried out in accordance with the IEEE Standard [19] on samples of porous piezoceramics, obtained using the same technological regimes. Porosity dependencies of dielectric, piezoelectric and electromechanical coefficients of the porous ceramics in the relative porosity range of 0–50% were obtained in the result of the analyses of measured piezoresonance spectra. The complex elastic, dielectric, and piezoelectric parameters of the piezoceramics elements were measured on standard samples using Agilent 4294A impedance analyzer and the piezoelectric resonance analysis (PRAP) software [20]. The frequency dependences of the complex parameters of the experimental samples in the frequency range up to 17 MHz were studied by analyzing the impedance spectra for the fundamental and higher-order resonances of thickness vibrational mode using the PRAP software [7, 21]. The developed technique allows measurements and analysis of the results in the high frequency ranges, for which the fabrication of porous piezoceramic elements, operating on the fundamental mode of thickness oscillations, is impossible because of a small thickness and fragility. To obtain a complete set of complex constants, the standard sets of samples of various shapes and sizes, and one-dimensional vibration modes relevant for the 6 mm symmetry class were used [22].

3 Results and Discussion

3.1 Microstructure Study

Micrographs, illustrating the main features of the porous piezoceramics microstructure, are shown in Figs. 1, 2, 3 and 4. According to the images, the porous piezoceramics are characterized by random distribution of irregular shape pores (dark spots in the gray piezoceramics matrix) with an average size of 10–30 μm.

With an increase in porosity, the appearance of larger branched pores, formed as result of the coalescence of neighboring smaller pores, is observed. We also noticed that at low porosity, the pores are mostly isolated, while at higher porosity the pores are interconnected.

The case of isolated pores corresponds to 3-0 connectivity while the interconnected pores case corresponds to 3-3 connectivity [23]. It can be seen from the micrographs that the ceramic skeleton is characterized by dense packing of grains with an average size of 3–5 μm that does not differ from the grain size, observed for dense piezoceramics of the same composition.

These micrographs demonstrate also the presence in porous piezoceramics of a rigid three-dimensional piezoceramics skeleton with continuous quasi-rod structure. The branched coral-type microstructure of porous ceramics determines the main features of its electromechanical properties.

3.2 Porosity Dependencies of Electromechanical Parameters

Figures 5, 6 and 7 show the dependences of the main electromechanical parameters of the studied porous piezoceramics on the relative porosity.

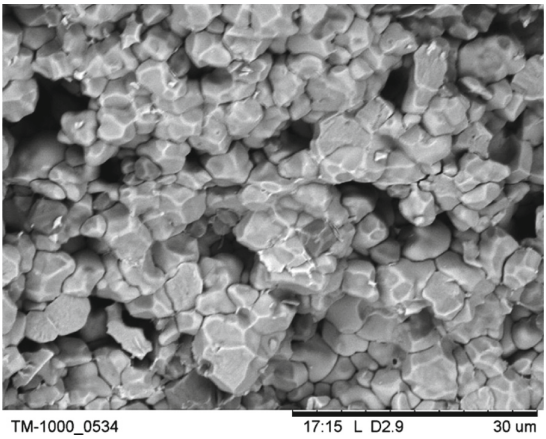

Fig. 1 SEM image of chipped surface of the porous piezoceramics with the relative porosity of 21%

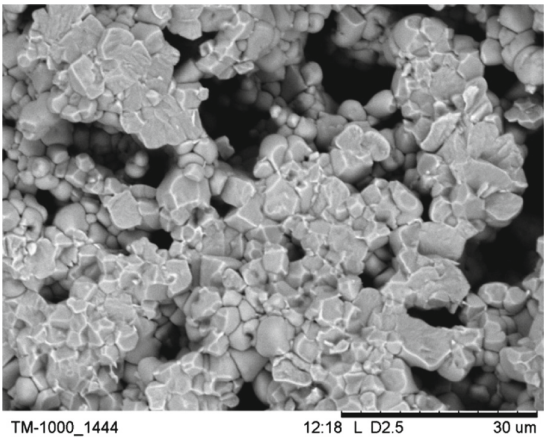

Fig. 2 Microstructure of the porous piezoceramics with the relative porosity of 29%

The dielectric constant of porous piezoceramics $\varepsilon_{33}^{T}/\varepsilon_0$ decreases almost linearly with porosity grows (Fig. 5), which is due to a significant difference in the dielectric constants of piezoelectric ceramics and air.

The dielectric loss tangent tgδ decreases slightly with porosity increase in the entire range of porosity values of $p \sim 0.5$ (Fig. 5) and approaches the initial value only at $p \sim 0.5$. A more developed internal surface of the porous piezoceramics contribute to the fixation of domain walls and lead to decrease in tgδ [13].

It should be noted that highly porous piezoceramics are hygroscopic, and correct measurements must be carried out at a controlled atmospheric humidity.

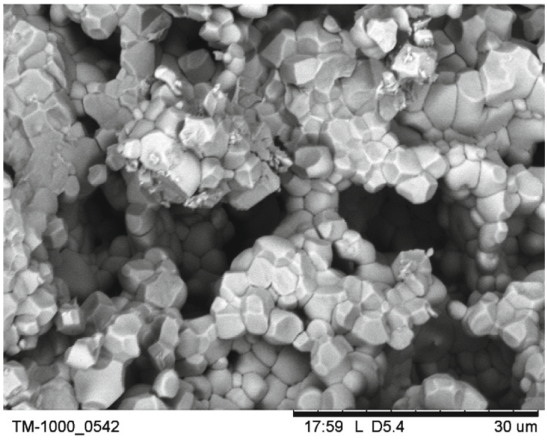

Fig. 3 Microstructure of the porous piezoceramics with the relative porosity of 41%

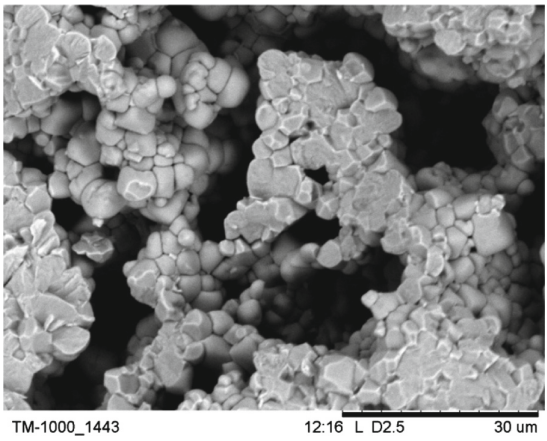

Fig. 4 Microstructure of the porous piezoceramics of the composition with the relative porosity of 49%

An increase in porosity p leads to noticeable changes in the piezoelectric moduli d_{33} and d_{31} of the porous piezoceramics (Fig. 6). A number of factors are responsible for the behavior of the piezoelectric moduli of porous piezoceramics.

The formation of continuous quasi-rod structure of porous piezoceramic in the direction of remnant polarization (Figs. 3 and 4) ensures the constancy of the piezoelectric modulus with porosity growth. A decrease in the surface area of the piezoelectric active phase is balanced by an increase in the specific pressure on the piezoceramics skeleton.

The growth of the piezoelectric modulus d_{33} of porous piezoceramics with the porosity is caused by the increased flex-tensional deformations of the branched three-dimensional piezoceramics skeleton (see Figs. 3 and 4) under the influence of external stress (direct piezoelectric effect) or electric field (inverse piezoelectric effect).

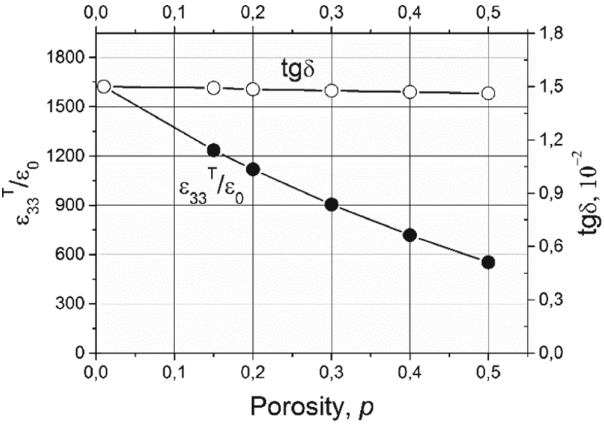

Fig. 5 Dependences of the dielectric constant $\varepsilon_{33}^T/\varepsilon_0$ and the loss tangent tgδ on the relative porosity p for the studied porous piezoceramics

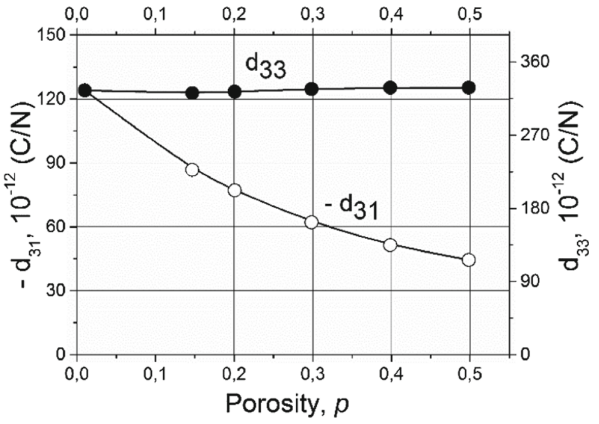

Fig. 6 Piezoelectric moduli d_{33} and $(-d_{31})$ as functions of the relative porosity p for the studied porous piezoceramics

Fast decrease in $|d_{31}|$ of porous ceramics with porosity growth (Fig. 6) is caused by the breach of the electromechanical connectivity of the non-uniformly polarized piezoceramics skeleton in the direction of remnant polarization and in the lateral directions.

The decrease in the electromechanical coupling factor k_{33} for length extensional mode of vibration for piezoceramics rod with porosity growth (Fig. 7) is caused by a rapid increase in the elastic compliance S_{33}^E of the porous piezoceramics skeleton ($k_{33}^2 = d_{33}^2/(\varepsilon_{33}^T S_{33}^E)$). A further decrease in k_{33} is prevented by the weakening of the mechanical clamping of the piezoceramics skeleton in the lateral direction in the result of the formation of a branched quasi-rod structure (see Figs. 3, 4 and 5).

The behavior of electromechanical coupling factor k_p for radial vibrational mode of thin piezoceramics disk at porosity growth (Fig. 7) is determined by competing

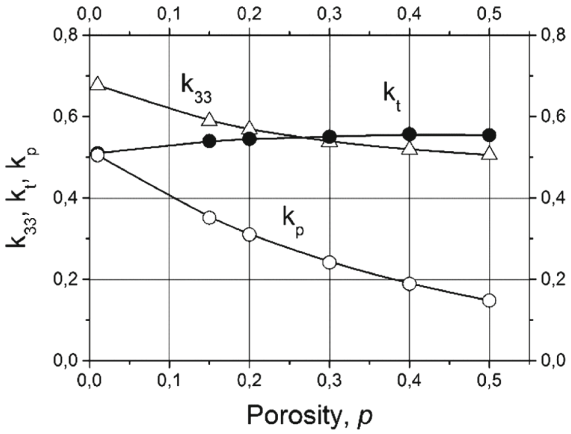

Fig. 7 Electromechanical coupling factors k_{33}, k_t and k_p as functions of the relative porosity p for the studied porous piezoceramics

influence of decrease in piezomodulus d_{31} and dielectric permittivity ${\varepsilon_{33}}^T$, and fast increase of elastic compliances ${S_{11}}^E$ and ${S_{12}}^E$ according to following relation: ${k_p}^{*2} = 2{d_{31}}^{*2}/[{\varepsilon_{33}}^T*({S_{11}}^E* + {S_{12}}^E*)]$. The main reason of k_p decrease is above mentioned breach of the electromechanical connectivity of the piezoceramic skeleton in the lateral direction and fast increase in corresponding elastic compliances of porous ceramics.

Significant increase in the electromechanical coupling factor k_t for thickness vibrational mode of thin piezoceramics disk at porosity growth (Fig. 7) and its approaching to the longitudinal electromechanical coupling factor k_{33}, is caused by the partial removal of the mechanical clamping of the quasi-rod piezoceramics skeleton in lateral direction, which is typical for dense piezoceramics. The relationship between the resulting values of the considered electromechanical coupling coefficients at any porosity is well described by an approximate relation: ${k_t}^2 \approx ({k_{33}}^2 + {k_p}^2)/(1 - {k_p}^2)$.

3.3 Complex Electromechanical Parameters

The complete set of complex dielectric, piezoelectric and elastic parameters of the porous piezoceramics with the relative porosity of 25% were measured on piezoceramic samples in the shape of disks, rods, and shear plates using the method developed in [24]. Impedance spectra, measured for radial, thickness, shear and longitudinal modes of the piezoceramic elements with the relative porosity of 25% are shown in Figs. 8, 9, 10 and 11.

Table 1 lists the complete piezoelectric matrices of the complex parameters of studied porous piezoceramics, obtained from the analysis of measured impedance spectra for four general representations of the 6 mm symmetry piezoelectric equations.

Figure 12 shows the impedance spectra and PRAP approximations for the first five harmonics of the thickness oscillation mode of the porous piezoceramic disks. It can be seen from Fig. 12 that each resonance peak of the higher order is clearly defined and

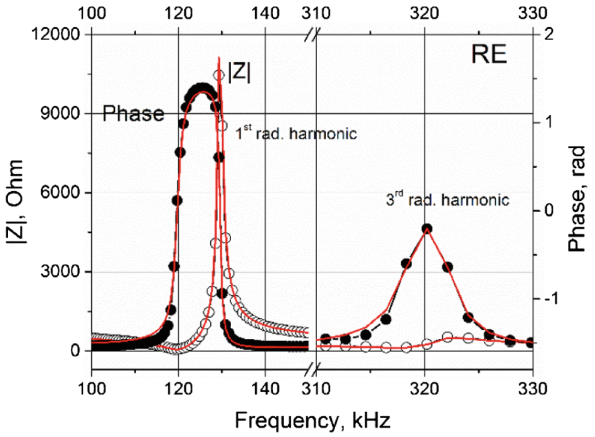

Fig. 8 Impedance spectrum for the radial extensional mode of the porous piezoceramic disk of 15 mm in diameter and 0.31 mm in thickness, polarized in the thickness direction

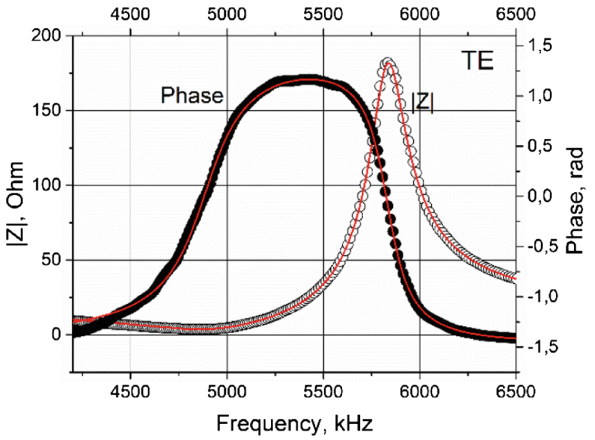

Fig. 9 Impedance spectrum for the thickness extensional mode of the porous piezoceramic disk of 15 mm in diameter and 0.31 mm in thickness, polarized in the thickness direction

allows one to perform PRAP analysis of the frequency dependences of the porous piezoceramics parameters in the frequency range up to 20 MHz at a fundamental resonance frequency of 2 MHz.

Figure 13 shows the frequency dependences of the real $C_{33}^{/D}$, $C_{33}^{/E}$ and imaginary $C_{33}^{//D}$, $C_{33}^{//E}$ parts of the elastic moduli of the porous piezoceramics, obtained by analyzing the impedance spectra for the fundamental and higher order harmonics of the thickness oscillation mode shown in Fig. 12.

As can be seen in Fig. 13, the real $C_{33}^{/E}$ and imaginary $C_{33}^{//E}$ parts of the elastic modulus C_{33}^{E} increase significantly with frequency, which is caused by the rapid growth

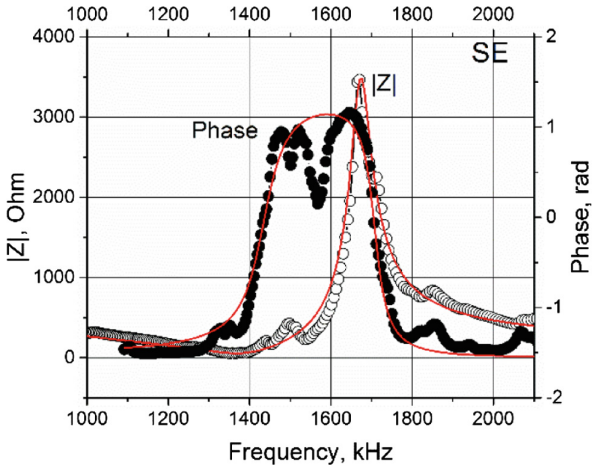

Fig. 10 Impedance spectrum for the shear vibrational mode of the porous piezoceramic plate of $7 \times 6 \times 0.6$ mm^3 in size, polarized in the width direction

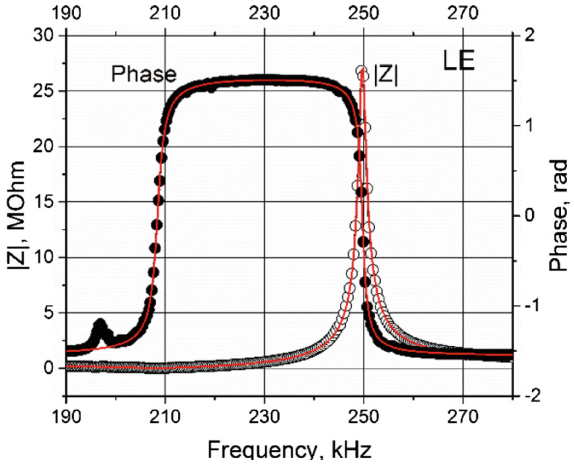

Fig. 11 Impedance spectrum for the length extensional mode of porous piezoceramic rod of $1.5 \times 1.5 \times 6$ mm^3 in size, polarized in the length direction

in the attenuation of ultrasonic waves in the result of Rayleigh scattering of elastic waves on pores ($\lambda >> D$, where λ is the wavelength and D is the average pore size).

The relationship between the attenuation coefficient $\alpha(\omega)$ and the dispersion of the phase velocity of elastic waves $dV(\omega)/d\omega$ in the small dispersion approximation has the following form [25]:

$$\alpha(\omega) = \frac{\pi\omega^2}{2V_0^2}\frac{dV(\omega)}{d\omega}$$

Table 1 Complex 6 mm piezoelectric matrix of the studied porous piezoceramics with the relative porosity of 25%

Parameter	Real	Imaginary	Parameter	Real	Imaginary
$S = S^D T + gD$ and $E = \beta^T D - gT$			$T = C^D S - hD$ and $E = \beta^D - hS$		
S_{11}^D (m^2/N)	2.16 × 10–11	-1.11×10^{-13}	C_{11}^D (N/m^2)	6.25×10^{10}	3.42×10^9
S_{12}^D (m^2/N)	-7.49×10^{-12}	1.72×10^{-14}	C_{12}^D (N/m^2)	2.82×10^{10}	3.27×10^9
S_{13}^D (m^2/N)	-5.35×10^{-12}	-5.55×10^{-13}	C_{13}^D (N/m^2)	2.7×10^{10}	5.24×10^9
S_{33}^D (m^2/N)	1.77×10^{-11}	-2.52×10^{-13}	C_{33}^D (N/m^2)	7.22×10^{10}	5.87×10^9
S_{55}^D (m^2/N)	3.59×10^{-11}	-1.91×10^{-12}	C_{55}^D (N/m^2)	2.78×10^{10}	1.48×10^9
S_{66}^D (m^2/N)	5.82×10^{-11}	-2.57×10^{-13}	C_{66}^D (N/m^2)	1.72×10^{10}	7.57×10^7
g_{15} (V·m/N)	0.0575	-2.47×10^{-3}	h_{15} (V/m)	1.6×10^9	1.66×10^7
g_{31} (V·m/N)	−0.0165	3.21×10^{-4}	h_{31} (V/m)	-2.77×10^8	1.76×10^8
g_{33} (V·m/N)	0.0453	7.21×10^{-4}	h_{33} (V/m)	2.37×10^9	1.63×10^8
β_{11}^T (m/F)	1.49×10^8	4.33×10^7	β_{11}^S (m/F)	2.41×10^8	4.03×10^7
β_{33}^T (m/F)	2.13×10^8	8.47×10^6	β_{33}^S (m/F)	3.3×10^8	1.16×10^7
$S = S^E T + dE$ and $D = \varepsilon^T + dT$			$T = C^E S - eE$ and $D = \varepsilon^T E + eS$		
S_{11}^E (m^2/N)	2.29 × 10–11	-2.11×10^{-13}	C_{11}^E (N/m^2)	6.24×10^{10}	3.72×10^9
S_{12}^E (m^2/N)	-6.21×10^{-12}	-8.3×10^{-14}	C_{12}^E (N/m^2)	2.8×10^{10}	3.57×10^9
S_{13}^E (m^2/N)	-8.85×10^{-12}	-4.04×10^{-13}	C_{13}^E (N/m^2)	2.91×10^{10}	4.04×10^9
S_{33}^E (m^2/N)	2.74×10^{-11}	-3.28×10^{-13}	C_{33}^E (N/m^2)	1.5×10^{11}	5.85×10^9
S_{55}^E (m^2/N)	5.58×10^{-11}	-9.63×10^{-12}	C_{55}^E (N/m^2)	1.74×10^{10}	3.0×10^9
S_{66}^E (m^2/N)	5.82×10^{-11}	-2.57×10^{-13}	C_{66}^E (N/m^2)	1.72×10^{10}	7.57×10^7
d_{15} (C/N)	3.52×10^{-10}	-1.19×10^{-10}	e_{15} (C/m^2)	6.48	−1.02
d_{31} (C/N)	-7.72×10^{-11}	4.57×10^{-12}	e_{31} (C/m^2)	−0.821	0.561
d_{33} (C/N)	2.12×10^{-10}	-5.06×10^{-12}	e_{33} (C/m^2)	7.21	0.241
ε_{11}^T (F/m)	6.2×10^{-9}	-1.81×10^{-9}	ε_{11}^S (F/m)	4.04×10^{-9}	-6.76×10^{-10}
ε_{33}^T (F/m)	4.68×10^{-9}	-1.86×10^{-10}	ε_{33}^S (F/m)	3.03×10^{-9}	-1.07×10^{-10}

$$\Delta V = V(\omega) - V_0 = \frac{2V_0^2}{\pi} \int_{\omega_0}^{\omega} \frac{\alpha(\omega')}{\omega'^2} d\omega',$$

where the sound velocity $V(\omega)$ is recorded as $V + \Delta V(\omega)$ at $\Delta V(\omega) \ll V_0$ and only terms of order $\Delta V(\omega)$ retain.

Since the frequency dependence of the sound velocity V_t^E is determined by the elastic modulus C_{33}^E, the growth of its real $C_{33}^{/E}$ and imaginary $C_{33}^{//E}$ parts in the Rayleigh region

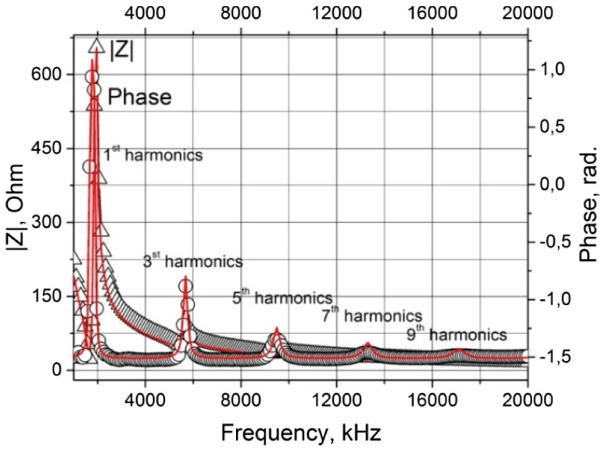

Fig. 12 Impedance spectra and PRAP approximations for the first five harmonics of the thickness oscillation mode of the porous piezoceramic disk Ø15 × 0.95 mm^2 with the relative porosity of 25%

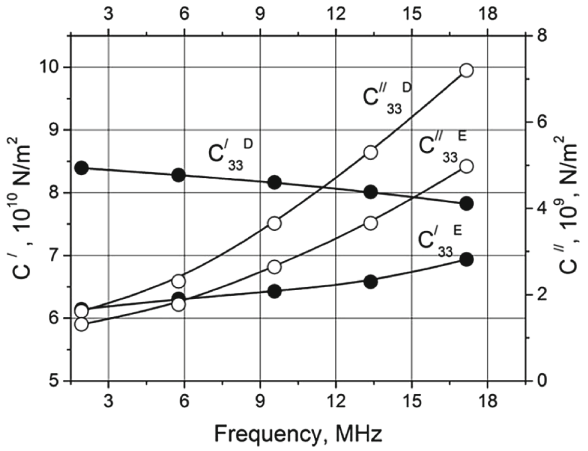

Fig. 13 Frequency dependences of the real $C_{33}^{/D}$, $C_{33}^{/E}$ and imaginary $C_{33}^{//D}$, $C_{33}^{//E}$ parts of complex elastic moduli of porous piezoceramic disk Ø15 × 0.95 mm^2 with the relative porosity of 25%

(normal type of dispersion) (Fig. 13) are in full agreement with theoretical predictions for the dispersion and attenuation of ultrasound in dissipative media [25].

In contrast, the real part of the elastic modulus $C_{33}^{/D}$ decreases (abnormal dispersion), and the imaginary part $C_{33}^{//D}$ increases with frequency. The difference in the behavior of the real parts of the elastic moduli $C_{33}^{/D}$ and $C_{33}^{/E}$ is caused by the frequency dependence of the electromechanical coupling coefficient of the thickness vibrational mode k_t, which contributes to the elastic modulus $C_{33}^{/E} = C_{33}^{/D}\left(1 - k_t^2\right)$. It should be noted, that the

effective value of k_t, measured at higher harmonics, decreases sharply with increasing harmonic number, according the relation: $k^2_{eff.n} = 8k_t^2/((2n+1)\pi)^2$ [26, 27].

The anomalous dispersion of the elastic properties of porous piezoceramics (a decrease in the elastic modulus $C_{33}^{/D}$ and the corresponding sound velocity V_t^D with increasing frequency) is due to its microstructural features, namely, the presence of a rigid three-dimensional piezoceramic frame and a quasi-rod structure (see Figs. 1, 2, 3 and 4).

4 Conclusions

In the result of SEM microstructure analysis, it was found that at any connectivity type (3-0, 3-3) and porosity up to 50%, the real structures of porous piezoceramics of the composition $PbTi_{0.45}Zr_{0.53}(W_{1/2}Cd_{1/2})_{0.02}O_3$ were close to the matrix medium structure with continuous coral-like piezoceramic skeleton.

It was revealed that the following microstructural features of the studied porous piezoceramics define the dielectric, piezoelectric and electromechanical properties of porous piezoelectric ceramics, branched flexible three-dimensional piezoceramics skeleton and quasi-rod piezoceramic structure in the direction of residual polarization of porous piezoceramics. Changes in the mechanical and electrical boundary conditions on the branched coral-like microstructure, as well as inhomogeneous polarization of the piezoceramic skeleton also play a significant role in the formation of electromechanical properties of the studied porous piezoelectric ceramics.

It was found that the porous piezoceramics similarly to 1–3 type composites are characterized by increased values of k_t and d_{33}, and reduced values of d_{31}, k_p, compared to dense piezoceramics, that makes they perspective materials for different ultrasonic applications in medical diagnostics and therapy, nondestructive testing, and active piezoelectric membranes for reverse osmosis, ultra- and microfiltration processes [28–30].

In the result of comprehensive studies of porous ferroelectric ceramics of the composition $PbTi_{0.45}Zr_{0.53}(W_{1/2}Cd_{1/2})_{0.02}O_3$ with the relative porosity of 25%, a complete set of complex elastic, dielectric, and piezoelectric parameters was obtained. The study of the frequency dependences of the complex elastic moduli C_{33}^E and C_{33}^D in the frequency range up to 17 MHz using the PRAP method allowed us to identify areas of normal and anomalous elastic dispersion in porous ferroelectric ceramics. Based on the analysis of general relationship between ultrasonic attenuation and dispersion, it was shown that the cause of the normal elastic dispersion in a porous piezoceramics is the rapid growth in the attenuation of ultrasonic waves with a frequency, caused by Rayleigh scattering of elastic waves in pores. In its turn, the anomalous dispersion of the elastic properties of the studied porous piezoceramics is due to its microstructural features, namely, the presence of a rigid three-dimensional piezoceramic frame and a quasi-rod structure.

Acknowledgement. The study was financially supported by the Russian Science Foundation, grant No. 22-11-00302, https://rscf.ru/project/22-11-00302/ at the Southern Federal University.

References

1. Topolov V, Bowen CR (2009) Electromechanical properties in composites based on ferroelectrics. Springer, London
2. Newton A (2017) Advances in porous ceramics. Nova Science Publishers, NY
3. Shvetsova NA, Petrova EI, Lugovaya MA, Marakhovsky MA, Bryl OE, Rybyanets AN (2022) Ferroelectrics 591(1):143. https://doi.org/10.1080/00150193.2022.2041932
4. Rybyanets AN (2011) Ferroelectrics 419(1):90. https://doi.org/10.1080/00150193.2011.594751
5. Wight J (2005) Cellular ceramics—structure, manufacturing, properties and applications. Wiley-VCH, Weinheim
6. Rybyanets AN (2010) In: Parinov IA (ed)Piezoceramic materials and devices, vol 113. Nova Science Publishers, NY
7. Rybyanets AN (2011) IEEE Trans Ultrason Ferroelectr Freq Control 58:1492. https://doi.org/10.1109/TUFFC.2011.1968
8. Rybyanets AN, Makarev DI, Shvetsova NA (2019) Ferroelectrics 539(1):101. https://doi.org/10.1080/00150193.2019.1570019
9. Pabst W, Gregorova E, Uhlifova T (2017) Processing, microstructure, properties, applications and curvature-based classification schemes of porous ceramics. Nova Science Publishers, NY
10. Studart AR, Gonzenbach UT, Tervoort E, Gauckler LJ (2006) J Am Ceram Soc 89:1771
11. Lee SH, Jun SH, Kim HE, Koh YH (2007) J Am Ceram Soc 90:2807
12. Rybyanets AN (2017) Advances in porous ceramics. Nova Science Publishers Inc., NY
13. Shvetsova NA, Shvetsov IA, Lugovaya MA, Petrova EI, Rybyanets AN (2022) J Adv Dielectr 12(2):2160006. https://doi.org/10.1142/S2010135X21600067
14. Bale A, Rouffaud R, Hladky-Hennion A-C, Marchet P, Levassort F (2019) IEEE Trans Ultrason Ferroelectr Freq Control 66(5), 8638828, 949. https://doi.org/10.1109/TUFFC.2019.2898519
15. Zeng T, Dong X, Mao C, Zhou Z, Yang H (2007) J Eur Ceram Soc 27:2025
16. Rybyanets AN, Naumenko AA, Lugovaya MA, Shvetsova NA (2015) Ferroelectrics 484(1):95
17. Ringgaard E, Lautzenhiser F, Bierregaard LM, Zawada T, Molz E (2015) Materials 8(12):8877. https://doi.org/10.3390/ma8125498
18. Shvetsov IA et al (2022) J Adv Dielectr 12(2):2160004–2160011. https://doi.org/10.1142/s2010135x21600043
19. IEEE Standard on Piezoelectricity (1987) ANSI/IEEE Std. 176
20. PRAP (Piezoelectric Resonance Analysis Program). TASI Technical Software Inc. www.tasitechnical.com
21. Lugovaya MA, Naumenko AA, Rybyanets AN, Shcherbinin SA (2015) Ferroelectrics 484(1):87. https://doi.org/10.1080/00150193.2015.1059723
22. Rybianets A, Kushkuley L, Eshel Y, Nasedkin A (2006) Proc IEEE Ultrason Symp 1(4152245):1533. https://doi.org/10.1109/ULTSYM.2006.389
23. Hudai K, Rajamami R, Stevens R, Bowen CR (2003) IEEE Trans. UFFC 50(3):289
24. Rybianets AN, Tasker R (2007) Ferroelectrics 360(1):90. https://doi.org/10.1080/00150190701516228
25. O'Donnell M, Jaynes ET, Miller JG (1978) J Acoust Soc Am 63:1935. https://doi.org/10.1121/1.381902
26. Rybyanets AN, Naumenko AA, Konstantinov GM, Shvetsova NA, Lugovaya MA (2015) Phys Solid State 57(3):558. https://doi.org/10.1134/S1063783415030269
27. Uchino K, Hirose S (2001) IEEE UFFC 48:307. https://doi.org/10.1109/58.896144

28. Lugovaya MA, Shvetsov IA, Shvetsova NA, Nasedkin AV, Rybyanets AN (2021) Ferroelectrics 571(1):263. https://doi.org/10.1080/00150193.2020.1736909
29. Rybyanets AN (2012) In: Parinov IA (ed) Piezoelectrics and related materials: investigations and applications, vol 143. Nova Science Publishers, New York
30. Rybianets A, Eshel Y, Kushkuley L (2006) Proceedings of the IEEE Ultrasonics Symposium IUS, vol 9474540. 1911. https://doi.org/10.1109/ULTSYM.2006.480